

CrossMark  
click for updatesCite this: *Chem. Sci.*, 2017, 8, 2776

# A new H<sub>2</sub>S-specific near-infrared fluorescence-enhanced probe that can visualize the H<sub>2</sub>S level in colorectal cancer cells in mice†

Kun Zhang,<sup>‡a</sup> Jie Zhang,<sup>‡b</sup> Zhen Xi,<sup>ac</sup> Lu-Yuan Li,<sup>a</sup> Xiangxiang Gu,<sup>a</sup>  
Qiang-Zhe Zhang<sup>\*a</sup> and Long Yi<sup>\*bc</sup>

Near-infrared (NIR) fluorescence-based sensors capable of selective detection of H<sub>2</sub>S *in vivo* would be useful tools to understand the mechanisms of diseases. A new NIR fluorescence probe **1** was developed for the detection of endogenous H<sub>2</sub>S in colorectal cancer cells in mice. **1** displayed an 87-fold fluorescence enhancement at 796 nm (with excitation at 730 nm) when reacted with H<sub>2</sub>S in a buffer (pH 7.4). **1** was water-soluble, cell-membrane-permeable, had low cytotoxicity and high selectivity and sensitivity for H<sub>2</sub>S. The properties of **1** enable its use in monitoring endogenous H<sub>2</sub>S in living cells, tissues, and mice. The bioimaging results indicated that (1) D-Cys could induce endogenous H<sub>2</sub>S production in living cells and stimulate angiogenesis; (2) tail intravenous injection of **1** into mice generated strong fluorescence in the liver while intraperitoneal injection of D-Cys could further enhance fluorescence in the liver *in vivo*; (3) importantly, endogenous H<sub>2</sub>S in colorectal cancer cells (HCT116, HT29) *in vitro* and in murine tumor models could be quickly and selectively detected by intratumoral injection of **1**. These results indicated that our new probe could serve as an efficient tool for the detection of cellular H<sub>2</sub>S in living animals and even for cancer diagnosis.

Received 23rd December 2016

Accepted 14th January 2017

DOI: 10.1039/c6sc05646f

rsc.li/chemical-science

## Introduction

Hydrogen sulfide (H<sub>2</sub>S) has long been known as a toxic gas, however recent studies indicated that endogenously produced H<sub>2</sub>S has important physiological functions, and was also named as the third gasotransmitter after nitric oxide and carbon monoxide.<sup>1</sup> Endogenous H<sub>2</sub>S can be enzymatically produced by three distinctive pathways including cystathionine β-synthase (CBS), cystathionine γ-lyase (CSE), and 3-mercaptopyruvate sulfurtransferase (3-MST) coupling with cysteine aminotransferase (CAT).<sup>2</sup> Accumulating evidence suggests that H<sub>2</sub>S influences a wide range of physiological and pathological processes,<sup>3–7</sup> including the modulation of blood vessel tone and

cardioprotection,<sup>3</sup> the endogenous stimulation of angiogenesis<sup>4</sup> and mitochondrial bioenergetics.<sup>5</sup> H<sub>2</sub>S inhibited nuclear factor-κB activation in oxidized low-density lipoprotein-stimulated macrophages.<sup>6</sup> H<sub>2</sub>S also plays important roles in tumor biology, and it is suggested that both the inhibition of H<sub>2</sub>S biosynthesis and elevation of H<sub>2</sub>S concentration beyond a certain threshold could exert anticancer effects.<sup>7,4b</sup> Nevertheless, the pharmacological character of H<sub>2</sub>S and the precise mechanisms by which H<sub>2</sub>S may be involved still remain largely unclear. Therefore, efficient tools for the visualization of endogenous H<sub>2</sub>S *in vivo* should be invaluable in further exploring H<sub>2</sub>S biology and even for the diagnosis of H<sub>2</sub>S-related diseases.

A fluorescence-based method has recently emerged as an efficient approach for the *in situ* and real-time detection of H<sub>2</sub>S in biological systems. Various fluorescence probes have been successfully employed to detect cellular H<sub>2</sub>S.<sup>8–16</sup> However, H<sub>2</sub>S fluorescence probes for *in vivo* bioimaging are still rare,<sup>8</sup> especially for the imaging of H<sub>2</sub>S-related diseases including cancers.<sup>11c</sup> Suitable fluorescence probes for the imaging of H<sub>2</sub>S in tissues or individuals are preferred to meet certain requirements, such as a NIR optical window, enhanced fluorescence, fast and sensitive response, good selectivity, water-solubility and low cytotoxicity simultaneously. Organic reactions of nucleophilic additions are not suitable for the development of turn-on NIR probes due to the interruption of a large conjugate system by H<sub>2</sub>S addition.<sup>10</sup> The reduction of a nitro group is relatively slow in a NIR probe,<sup>12c</sup> while azide-based NIR probes

<sup>a</sup>State Key Laboratory of Medicinal Chemical Biology and College of Pharmacy, Tianjin Key Laboratory of Molecular Drug Research, Nankai University, Tianjin 300071, China. E-mail: zhangqiangzhe@nankai.edu.cn

<sup>b</sup>State Key Laboratory of Organic-Inorganic Composites and Beijing Key Laboratory of Energy Environmental Catalysis, Beijing University of Chemical Technology (BUCT), 15 Beisanhuan East Road, Chaoyang District, Beijing 100029, China. E-mail: yilong@mail.buct.edu.cn

<sup>c</sup>State Key Laboratory of Elemento-Organic Chemistry, National Engineering Research Center of Pesticide (Tianjin), Collaborative Innovation Center of Chemical Science and Engineering, Nankai University, Tianjin 300071, China

† Electronic supplementary information (ESI) available: Experimental details, photophysical data, some fluorescence imaging figures, average fluorescence intensity figures and *in vivo* imaging. See DOI: 10.1039/c6sc05646f

‡ These authors contributed equally to this work.



are not employed for the imaging of  $\text{H}_2\text{S}$  in animals.<sup>12</sup> Thiolytic reactions should be one of ideal strategies for the development of NIR probes. Considering the concentration of GSH ranges from 1 to 15 mM depending on the cell types,<sup>17</sup> we discovered a reaction of  $\text{H}_2\text{S}$ -specific thiolytic of 7-nitro-1,2,3-benzoxadiazole (NBD) amines even in the presence of millimolar GSH,<sup>16</sup> which was further employed herein for the development of a new NIR probe **1** (Scheme 1).

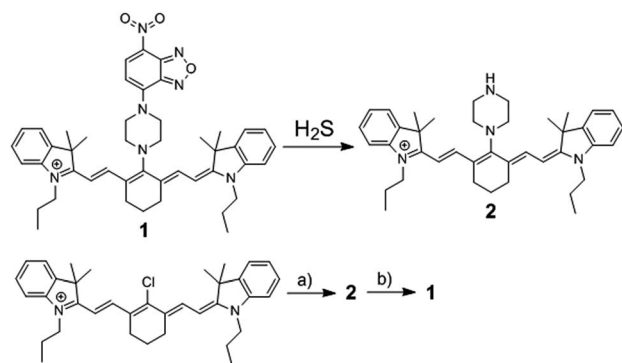
NIR light, especially at 700–900 nm, can improve the tissue depth penetration, offer low phototoxicity to cells and minimize the effect from background autofluorescence.<sup>18</sup> Among NIR fluorochromes, cyanine dyes have excellent photophysical properties, outstanding biocompatibility, and low toxicity to living systems for the successful development of fluorescence probes.<sup>19</sup> Herein we report a cyanine-based NIR probe **1** for the highly selective imaging of endogenous  $\text{H}_2\text{S}$  in tissues and living mice. We also successfully applied probe **1** for monitoring intratumoral  $\text{H}_2\text{S}$  by an *in vivo* fluorescence bioimaging technique, highlighting the potentially tumor-diagnostic value of this NIR probe.

## Results and discussion

### Synthesis and optical characterizations

The reaction of commercially available Cy7-Cl and piperazine in DMF provided **2**,<sup>19b</sup> and the synthesis of **1** was easily achieved by coupling reaction of **2** and NBD-Cl (Scheme 1). A facile and economic synthesis is important for the wide use of such a probe. **1** was well characterized by  $^1\text{H}$  NMR,  $^{13}\text{C}$  NMR and HRMS.

Studies were carried out to use **1** for the detection of  $\text{H}_2\text{S}$  under simulated physiological conditions (50 mM phosphate buffer saline (PBS), pH 7.4). The time-dependent absorbance (Fig. S1†) at NIR range for **1** exhibited a maximum at 700 nm, which shifted to around 740 nm after treatment with  $\text{H}_2\text{S}$ . The NBD absorbance displayed a decrease at 450–500 nm and an increase at 565 nm, implying that  $\text{H}_2\text{S}$  could cleave the NBD moiety from probe **1** to give **2**. This was further supported by the HRMS results of **1**, exhibiting a peak at  $m/z = 589.4268$  after treatment with  $\text{H}_2\text{S}$ , which corresponded to **2** ( $[\text{M}^+]$  589.4265).



**Scheme 1** The chemical structure of fluorescence probe **1**, its reaction with  $\text{H}_2\text{S}$ , and its synthetic routine. (a) Piperazine, 82.3%; (b) 7-nitro-1,2,3-benzoxadiazole chloride, 60.2%.

The absorbance of probe **1** at 700 nm exhibited a wide linear range in 2% DMSO-containing PBS (Fig. S2†), indicating that the probe had good water-solubility up to over 100  $\mu\text{M}$ .

The fluorescence of probe **1** was checked in the absence and presence of  $\text{H}_2\text{S}$  in PBS buffer (pH 7.4) (Fig. 1, 2 and S3–S8†). The excitation spectrum of probe **1** in the presence of  $\text{H}_2\text{S}$  indicated multiple peaks (689 nm, 714 nm, 733 nm and 764 nm) in the NIR range, providing flexibility for choosing excitation conditions in the NIR range. As shown in Fig. 1, the emission of probe **1** was nearly completely quenched at 796 nm. It is possible that electron transfer might occur from the NBD recognition unit to the cyanine group, resulting in quenching of the fluorophore, which is called the PET (photo-induced electron transfer) effect.<sup>20</sup> After reacting with  $\text{H}_2\text{S}$  at 37 °C, the NBD part is moved, and hence the PET effect disappears, resulting in the recovery of fluorescence emission of the NIR cyanine. The titration experiments indicated that a higher  $\text{H}_2\text{S}$  concentration induced a larger turn-on fluorescence response (Fig. 1), with an off-on response up to 87-fold higher at 796 nm. Further data analysis revealed an excellent linear relationship ( $r = 0.994$ ) between the fluorescence signal at 796 nm and the concentration of  $\text{H}_2\text{S}$  (3–20  $\mu\text{M}$ ). We further titrated a low-millimolar concentration of  $\text{H}_2\text{S}$  toward the probe **1** at 37 °C and determined a detection limit of 39.6 nM (Fig. S5†) by the  $3\sigma/k$  method,<sup>21</sup> indicating the high sensitivity of our probe. To obtain the reaction kinetics, the time-dependent fluorescence at 796 nm was recorded for data analysis (Fig. S6–S8†). The thiolytic rate for **1** by  $\text{H}_2\text{S}$  was found to be up to 14.9  $\text{M}^{-1} \text{s}^{-1}$  at 37 °C. These results implied that probe **1** could react with  $\text{H}_2\text{S}$  both sensitively and efficiently.

A major challenge for  $\text{H}_2\text{S}$  detection in biological systems is to develop a highly selective probe that exhibits a distinctive response to micromolar  $\text{H}_2\text{S}$  concentrations over millimolar GSH concentrations. Probe **1** was incubated with various biological-related species in PBS buffer for 30 min and the maximum emission change at 796 nm was measured accordingly (Fig. 2). The tested species included reactive sulfur species (GSH, 5 mM; Cys, 1 mM; Hcy, 1 mM), reactive oxygen species ( $\text{H}_2\text{O}_2$ ,  $\text{ClO}^-$ ), additional reactive sulfur species ( $\text{SO}_3^{2-}$ ,  $\text{S}_2\text{O}_3^{2-}$ ), anions ( $\text{NO}_2^-$ ), cations ( $\text{Zn}^{2+}$ ,  $\text{Fe}^{3+}$ ), low-molecular weight

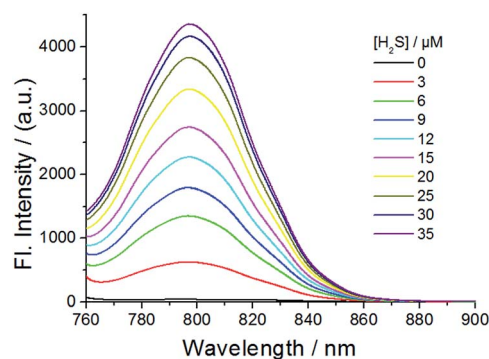


**Fig. 1** Emission spectra of probe **1** (10  $\mu\text{M}$ ) in the presence of various concentrations of  $\text{H}_2\text{S}$  at 37 °C for 30 min in PBS buffer (50 mM, pH 7.4). Excitation, 730 nm.



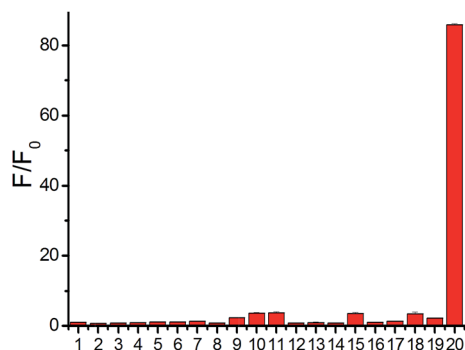


Fig. 2 Relative fluorescence intensity at 796 nm of probe **1** (10  $\mu$ M) with various species at 37  $^{\circ}$ C for 30 min in PBS buffer. Lane 1, only probe; lane 2, 100  $\mu$ M  $\text{Fe}^{3+}$ ; lane 3, 100  $\mu$ M  $\text{Zn}^{2+}$ ; lane 4, 100  $\mu$ M  $\text{H}_2\text{O}_2$ ; lane 5, 100  $\mu$ M  $\text{ClO}^-$ ; lane 6, 100  $\mu$ M  $\text{NO}_2^-$ ; lane 7, 100  $\mu$ M  $\text{S}_2\text{O}_3^{2-}$ ; lane 8, 100  $\mu$ M  $\text{SO}_3^{2-}$ ; lane 9, 1 mM Hcy; lane 10, 1 mM Cys; lane 11, 5 mM GSH; lane 12, 1 mM 2,2'-dithiodipyridine; lane 13, 1 mM 2,2'-dithiodipyridine + 100  $\mu$ M  $\text{H}_2\text{S}$ ; lane 14, 1 mM cystamine; lane 15, 1 mM cystamine + 100  $\mu$ M  $\text{H}_2\text{S}$ ; lane 16, 10  $\mu$ M lysozyme; lane 17, 10  $\mu$ M lysozyme + 100  $\mu$ M dithiodipyridine + 50  $\mu$ M  $\text{H}_2\text{S}$ ; lane 18, 10  $\mu$ M BSA; lane 19, 10  $\mu$ M BSA + 100  $\mu$ M dithiodipyridine + 50  $\mu$ M  $\text{H}_2\text{S}$ ; lane 20, 100  $\mu$ M  $\text{H}_2\text{S}$ .

species and protein persulfides.<sup>22</sup> The fluorescence intensity enhancement for any tested molecule in PBS buffer (pH 7.4) was very small except for  $\text{H}_2\text{S}$  (Fig. 2), indicating the high selectivity of our NIR probe.<sup>15</sup>

### Fluorescence imaging of $\text{H}_2\text{S}$ in living cells by **1**

To test the biological applicability of the NIR probe, we firstly examined whether it can be used to detect  $\text{H}_2\text{S}$  in living cells. Herein, mouse endothelial cell line (bEnd.3, with a low background endogenous  $\text{H}_2\text{S}$  level) was employed for studying  $\text{H}_2\text{S}$ -related angiogenesis.<sup>4</sup> The results indicated that the **1**-treated cells (bEnd.3) showed weak fluorescence while the addition of both probe **1** and  $\text{H}_2\text{S}$  to the cells resulted in obvious fluorescence, and a higher  $\text{H}_2\text{S}$  concentration induced stronger fluorescence (Fig. S9<sup>†</sup>), implying that **1** could be used for the visualization of a change in  $\text{H}_2\text{S}$  levels. The control experiments of aminooxyacetic acid (AOAA)-pretreated cells showed much weaker fluorescence than that of cells in the absence of an inhibitor (Fig. S10<sup>†</sup>), implying that **1** could be used for the detection of endogenous  $\text{H}_2\text{S}$  in cells lines with a low background  $\text{H}_2\text{S}$  level. Bright-field images show that cells retained a good morphology after incubation with **1**, suggesting good biocompatibility with the probe. The biocompatibility of **1** was further evaluated using cells by MTT assay (Fig. S11<sup>†</sup>). The results indicated that the probe possesses low cytotoxicity at the test concentration.

To test whether **1** could detect endogenous production of  $\text{H}_2\text{S}$  in living cells, we employed D-Cys as a stimulant because our previous work indicated that D-Cys can induce enzymatic  $\text{H}_2\text{S}$  production in mitochondria from HEK293 cells.<sup>16a</sup> Cells with **1** displayed weak fluorescence, while in the D-Cys-stimulated cells strong fluorescence could be observed (Fig. 3a–c), implying that D-Cys induced endogenous  $\text{H}_2\text{S}$  production. The

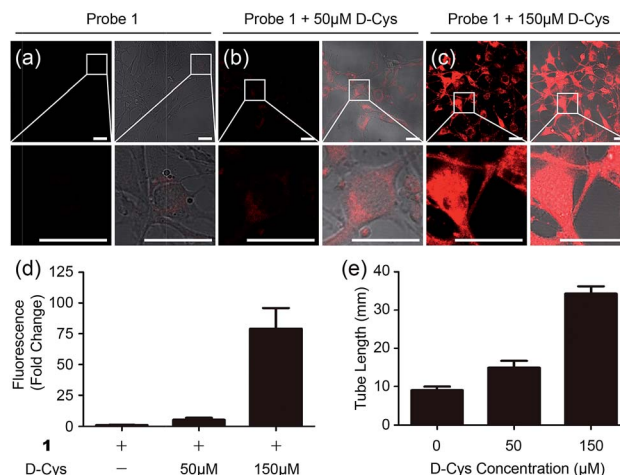


Fig. 3 Microscope images of D-Cys-induced  $\text{H}_2\text{S}$  in living cells and the angiogenesis assay in the presence of D-Cys. (a–c) Fluorescence images and overlap pictures of fluorescence and bright-field images of cells with 10  $\mu$ M of probe **1**, with 50  $\mu$ M of D-Cys and then 10  $\mu$ M of probe, with 150  $\mu$ M of D-Cys and then 10  $\mu$ M of the probe, respectively. Scale bar, 25  $\mu$ m. (d) The average fluorescence intensity of fluorescence images in panels (a–c). (e) Quantitative tube length at indicated D-Cys concentrations in Fig. S12<sup>†</sup>.

average fluorescence of the images (Fig. 3d) implied that a higher concentration of D-Cys induced more  $\text{H}_2\text{S}$  production in cells, and such an effect was further employed for the *in vitro* angiogenesis assay in the presence of D-Cys (Fig. S12<sup>†</sup>). The results indicated the tube length of the 50  $\mu$ M D-Cys treated group became about 1.5-fold higher than that of the vehicle-treated group, while the 150  $\mu$ M D-Cys treated group increased 2.5-fold (Fig. 3e). Therefore, D-Cys could induce endogenous  $\text{H}_2\text{S}$  production in living cells and stimulate angiogenesis, which has not been observed previously. Taken together, these results indicated that probe **1** can be used for the study of endogenous  $\text{H}_2\text{S}$  production and its biological functions.

### *In vivo* fluorescence imaging of $\text{H}_2\text{S}$ in mice by **1**

The high selectivity and excitation/emission wavelength of **1** in the NIR range shows it should be suitable for visualization of endogenous  $\text{H}_2\text{S}$  *in vivo*. We firstly examined the suitability of **1** for visualizing exogenous  $\text{H}_2\text{S}$  in mice. Mice were intraperitoneally (i.p.) cavity injected with probe **1** and  $\text{Na}_2\text{S}$ , and then imaged using Xenogen IVIS Spectrum (IVIS Lumina II), a small animal *in vivo* imaging system with a 710 nm excitation filter and an ICG emission filter. The results (Fig. S13 and S14<sup>†</sup>) indicated that the mouse treated with both  $\text{Na}_2\text{S}$  and the probe displayed much higher fluorescence than that treated only with the probe, and time-dependent images showed that the fluorescence response *in vivo* was fast with a  $t_{1/2}$  of less than 10 min, which is comparable with *in vitro* kinetic studies (Fig. S8<sup>†</sup>). The results indicated that the NIR probe possessed a desirable penetration depth for *in vivo* imaging, and could be further used to investigate endogenous  $\text{H}_2\text{S}$  in living mice and tissues.

As shown in Fig. 4, the mice in group a were intravenously injected with probe **1** for 0–30 min, and intense time-dependent





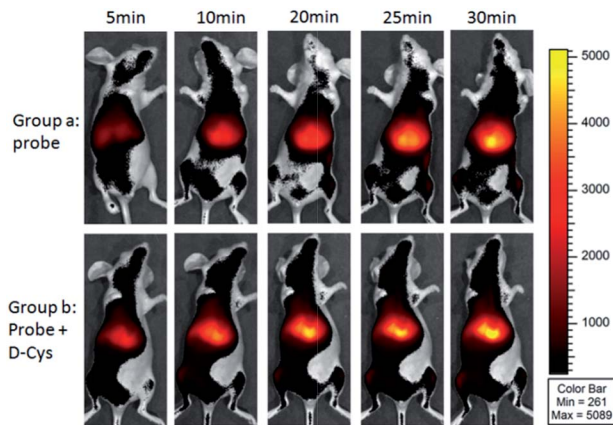


Fig. 4 Representative fluorescence images for visualizing endogenous  $\text{H}_2\text{S}$  with tail intravenous injection of probe 1 (150  $\mu\text{M}$ , 200  $\mu\text{L}$ ) in living mice. For group a, time-dependent images of a mouse *via* only injection of probe 1; for group b, time-dependent images of a mouse *via* i.p. injection of D-Cys, and after 30 min tail intravenous injection of probe 1.

enhanced fluorescence could be observed in the liver of living mice. We also investigated the D-Cys-induced  $\text{H}_2\text{S}$  in living mice with probe 1. The mice in group b were i.p. injected with D-Cys. After 30 min, the mice were intravenously injected with probe 1. A time-dependent fluorescence increase in the liver was also observed (Fig. 4). The average fluorescence of group b was about 10–20% higher than that of group a at various time points (Fig. S15<sup>†</sup>), implying that D-Cys could be metabolized into  $\text{H}_2\text{S}$  in living mice and greatly occurred in the liver. These results were further confirmed by tissue imaging from the intravenous injection in mice (Fig. S16<sup>†</sup>). Fluorescence imaging indicated that  $\text{H}_2\text{S}$  was produced in the tissues of the liver and the kidney, with the fluorescence intensity of the liver being larger than that of the kidney. While in the case of D-Cys-induced  $\text{H}_2\text{S}$ , stronger fluorescence was observed for both liver and kidney tissues than that of the uninduced mice. The western blotting results indicated that the  $\text{H}_2\text{S}$ -produced enzymes (e.g. CBS) in the liver are more expressed than that of the kidney (Fig. S16F<sup>†</sup>), which is consistent with our fluorescence imaging results. Similar results of endogenous  $\text{H}_2\text{S}$  in the liver were also observed with the injection of a lower amount of probe 1 in another group of mice (Fig. S17 and S18<sup>†</sup>). These observations clearly demonstrate that 1 is an effective probe for endogenous  $\text{H}_2\text{S}$  at the organism level.

### Fluorescence imaging of endogenous $\text{H}_2\text{S}$ in cancer cells and in mice by 1

Importantly, we hope to use the NIR  $\text{H}_2\text{S}$  probe to image  $\text{H}_2\text{S}$ -related cancers *in vivo*. Herein human colorectal epithelial cancer cell lines HCT116 and HT29 were selected as model biological systems and human normal colorectal epithelial cell line FHC was used as a control.<sup>7c</sup> We tested the fluorescence images of these cell lines with probe 1 (Fig. 5a and S19<sup>†</sup>). The results indicated that the 1-treated cancer cells (HCT116 or HT29) showed stronger fluorescence than that of the FHC cells.

The control experiments of  $\text{ZnCl}_2$ -pretreated cells showed nearly no fluorescence for all cell lines. Changes of the endogenous  $\text{H}_2\text{S}$  level in living cells by inhibitors AOAA or siRNA were further performed by the gene-knockdown-based fluorescence imaging strategy from our previous work.<sup>11d,23</sup> Normal cells and specific gene-silencing cells were used for the bioimaging of endogenous  $\text{H}_2\text{S}$  with probe 1 (Fig. S20<sup>†</sup>). The fluorescence of AOAA-treated or siRNA-treated cells was significantly weaker than that of the corresponding untreated cells (Fig. 5b and c). The mRNA expression level of  $\text{H}_2\text{S}$ -produced enzymes of all cell lines and siRNA-silenced cells were checked by quantitative real-time PCR (Fig. 5d). The results indicated that both cancer cells (HCT116, HT29) expressed more  $\text{H}_2\text{S}$ -produced enzymes, CBS and CSE, than that of the control cells (FHC), which explained the higher  $\text{H}_2\text{S}$  level in cancer cells from our fluorescence imaging results. The expression of the  $\text{H}_2\text{S}$ -produced enzymes could be downregulated *via* RNAi to give a low endogenous  $\text{H}_2\text{S}$  level in living cancer cells, which could be visualized by our NIR probe.

Now that probe 1 could detect endogenous  $\text{H}_2\text{S}$  in colorectal cancer cells, imaging of intratumoral  $\text{H}_2\text{S}$  *in vivo* was further tested. FHC, HCT116, and HT29 cells were grafted into the nude mouse, respectively, to produce murine xenograft tumor models. After the direct skin-pop (s.p.) injection of 1 in PBS buffer into the tumors of HCT116- or HT29-xenograft mice, the emission was collected in the NIR range. Control experiments contained (1) the s.p. injection of 1 into other nontumoral parts of the same mice and (2) a FHC-xenograft mice (Fig. 5e). To kinetically observe the change in the fluorescence intensity, time-dependent experiments were performed (Fig. 5f, S21 and S22<sup>†</sup>). The results indicated that strong fluorescence in the tumor part could be observed quickly after intratumoral injection (5 min), while the control experiments only showed very weak fluorescence under the same conditions. Time-dependent fluorescence intensity measurements of these mice (Fig. 5d) indicated that the fluorescence of HCT116 and HT29 xenograft tumors is much higher than that of other parts (C1–C3, T1). Pre-injection of inhibitor AOAA significantly decreased the intratumoral fluorescence (Fig. S23<sup>†</sup>). Considering that  $\text{H}_2\text{S}$  could be a biomarker in CBS- or CSE-overexpressed cancer cells (colorectal and ovarian cancers),<sup>7c</sup> we proposed that our probe 1 combined with fluorescence bioimaging in the NIR range could provide a potential tool for the *in vivo* monitoring of endogenous  $\text{H}_2\text{S}$  in the tumor. To our knowledge, this is the first time a NIR probe has been used for the monitoring of  $\text{H}_2\text{S}$  in tumors *in vivo*.<sup>24</sup>

Moreover, we used the NIR probe to test the detection limit of colorectal cancer cells *in situ* in living mice (Fig. 6). Mice were injected with different numbers of HT29 cells and the probe was used to image the cancer cells at 24 h after injection. A significant fluorescence signal was detected in the cell-injected region even at 5 min for  $10^7$  cancer cells. After 30 min, a strong fluorescence signal could be observed for  $10^3$  to  $10^7$  HT29 cells in living mice, and the signal intensity for  $10^3$  cells was stronger than that for the PBS control (Fig. S24<sup>†</sup>). Taking the results from the *in vitro* and *in vivo* experiments together, we believe that the NIR probe is highly sensitive for



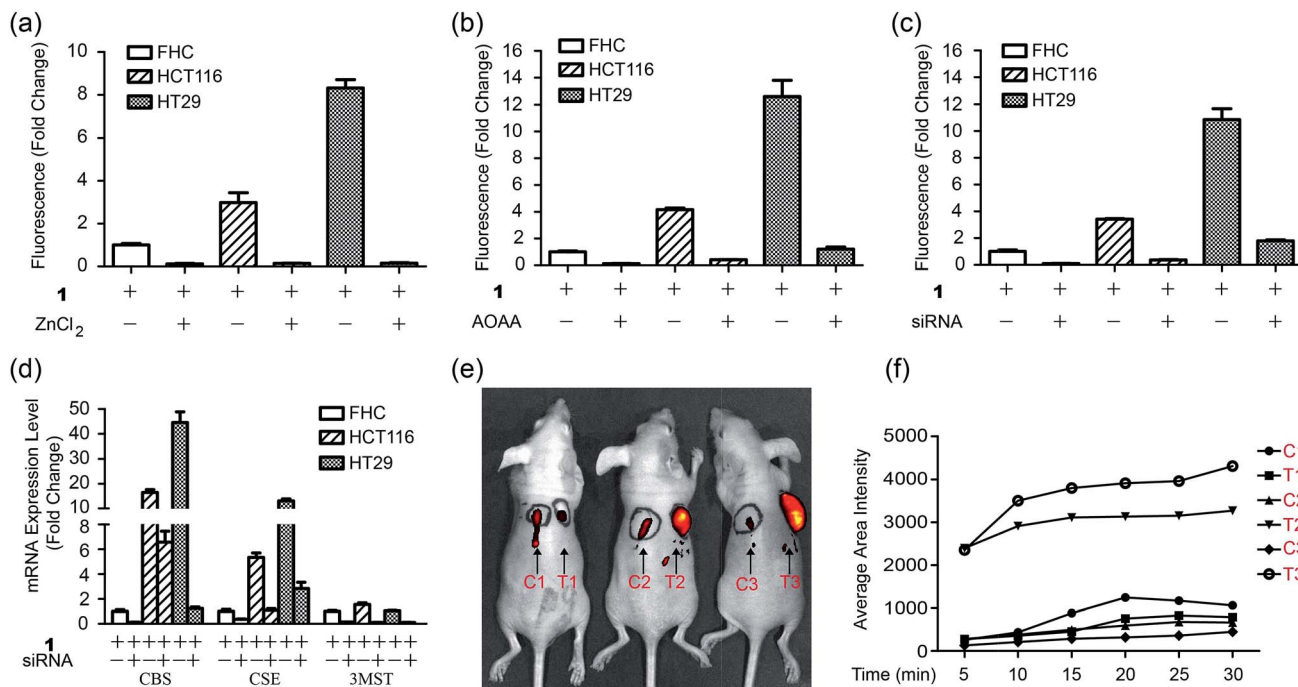


Fig. 5 Fluorescence imaging of endogenous  $\text{H}_2\text{S}$  in CBS-overexpressed cancer cells in mice. (a) Average fluorescence of images of living cells (FHC, HCT116, HT29) in the presence or absence of  $\text{ZnCl}_2$ . (b) Average fluorescence of images of living cells in the presence or absence of inhibitor AOOA. (c) Average fluorescence of images of living cells in the presence or absence of siRNAs. (d) The mRNA expression level for  $\text{H}_2\text{S}$ -produced enzymes in three cell lines in the presence or absence of siRNAs. (e) *In vivo* fluorescence images of mice with skin-pop (s.p.) or intratumoral injection of probe 1. The left injection positions (C1, C2, C3) were for control purposes, while the right injection positions (T1, T2, T3) were for FHC, HCT116, and HT29 grafted cell positions. Observed tumors were formed in the HCT116 (T2) and HT29 (T3) xenograft mice. (f) The time-dependent average fluorescence of C1–C3, T1–T3 positions in mice in panel (e).

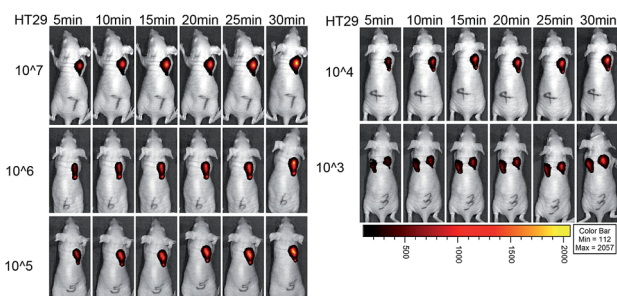


Fig. 6 Cancer cell detection limit and sensitivity of the NIR probe in living mice. Fluorescence images of mice with injection of  $10^7$ ,  $10^6$ ,  $10^5$ ,  $10^4$  and  $10^3$  HT29 cells at different time points. The control of only the PBS-injected position was in the left part of the mouse which was injected with  $10^3$  HT29 cells in the right part.

imaging endogenous  $\text{H}_2\text{S}$  in cancer cells and in mice with an excellent detection limit.

## Conclusions

In summary, we have developed a new NIR fluorescence probe 1 capable of real-time imaging of endogenous  $\text{H}_2\text{S}$  in cells, tissues (containing tumors) and mice. 1 is highly selective, has enhanced fluorescence (87-fold), a fast-response, is water soluble and has a low cytotoxicity with both an excitation and

emission larger than 700 nm. The properties of 1 enable its use for noninvasive *in vivo* imaging of endogenous  $\text{H}_2\text{S}$  without interfering with biological autofluorescence. Fluorescence imaging combined with the tail intravenous injection of 1 revealed that endogenous  $\text{H}_2\text{S}$  heavily existed in the liver of living mice and D-Cys could induce more  $\text{H}_2\text{S}$  production in the liver *in vivo*. Moreover, the endogenous  $\text{H}_2\text{S}$  in colorectal cancer cells and in the tumors of mice could be detected by our probe tool. This new probe could serve as an efficient tool for the detection of cellular  $\text{H}_2\text{S}$  in living animals and even for tumor diagnosis.

## Acknowledgements

This work was supported by NSFC (21332004, 21402007, 81272356, 81672747), the Fundamental Research Funds for the Central Universities (YS1401) and Tianjin Municipality Science and Technology Commission (15JCYBJC50100).

## Notes and references

- (a) R. Wang, *Physiol. Rev.*, 2012, **92**, 791; O. Kabil and R. Banerjee, *Antioxid. Redox Signaling*, 2014, **20**, 770. (b) G. K. Kolluru, X. Shen, S. C. Bir and C. G. Kevil, *Nitric Oxide*, 2013, **35**, 5.



- 2 L. Li, P. Rose and P. K. Moore, *Annu. Rev. Pharmacol. Toxicol.*, 2011, **51**, 169.
- 3 Y. H. Liu, M. Lu, L. F. Hu, P. T. Wong, G. D. Webb and J. S. Bian, *Antioxid. Redox Signaling*, 2012, **17**, 141.
- 4 (a) A. Papapetropoulos, A. Pyriochou, Z. Altaany, G. Yang, A. Marazioti, Z. Zhou, M. G. Jeschke, L. K. Branski, D. N. Herndon, R. Wang and C. Szabó, *Proc. Natl. Acad. Sci. U. S. A.*, 2009, **106**, 21972; (b) C. Coletta, K. Módis, B. Szczesny, A. Brunyánszki, G. Oláh, E. CS Rios, K. Yanagi, A. Ahmad, A. Papapetropoulos and C. Szabo, *Mol. Med.*, 2015, **21**, 1.
- 5 K. Módis, Y. Ju, A. Ahmad, A. A. Untereiner, Z. Altaany, L. Wu, C. Szabó and R. Wang, *Pharmacol. Res.*, 2016, **113**, 116.
- 6 J. Du, Y. Huang, H. Yan, Q. Zhang, M. Zhao, M. Zhu, J. Liu, S. X. Chen, D. Bu, C. Tang and H. Jin, *J. Biol. Chem.*, 2014, **289**, 9741.
- 7 (a) C. Szabo, *Nat. Rev. Drug Discovery*, 2016, **15**, 185; (b) D. Wu, W. Si, M. Wang, S. Lv and A. Ji, *Nitric Oxide*, 2015, **50**, 38; (c) M. R. Hellmich, C. Coletta, C. Chao and C. Szabo, *Antioxid. Redox Signaling*, 2015, **22**, 424.
- 8 For selected reviewers: (a) V. S. Lin, W. Chen, M. Xian and C. J. Chang, *Chem. Soc. Rev.*, 2015, **44**, 4596; (b) F. B. Yu, X. Y. Han and L. X. Chen, *Chem. Commun.*, 2014, **50**, 12234.
- 9 (a) Y. Qian, J. Karpus, O. Kabil, S. Y. Zhang, H. L. Zhu, R. Banerjee, J. Zhao and C. He, *Nat. Commun.*, 2011, **2**, 495; (b) L. W. He, W. Y. Lin, Q. Y. Xu and H. P. Wei, *Chem. Commun.*, 2015, **51**, 1510; (c) Y. Qian, L. Zhang, S. T. Ding, X. Deng, C. He, X. E. Zheng, H. L. Zhu and J. Zhao, *Chem. Sci.*, 2012, **3**, 2920; (d) X. Feng, T. Zhang, J.-T. Liu, J.-Y. Miao and B.-X. Zhao, *Chem. Commun.*, 2016, **52**, 3131.
- 10 (a) Y. C. Chen, C. C. Zhu, Z. H. Yang, J. J. Chen, Y. F. He, Y. Jiao, W. J. He, L. Qiu, J. J. Cen and Z. J. Guo, *Angew. Chem., Int. Ed.*, 2013, **52**, 1688; (b) X. Wang, J. Sun, W. Zhang, X. Ma, J. Lv and B. Tang, *Chem. Sci.*, 2013, **4**, 2551; (c) H. D. Li, Q. C. Yao, J. L. Fan, N. Jiang, J. Y. Wang, J. Xia and X. J. Peng, *Chem. Commun.*, 2015, **51**, 16225.
- 11 (a) L. Zhang, W. Q. Meng, L. Lu, Y. S. Xue, C. Li, F. Zou, Y. Liu and J. Zhao, *Sci. Rep.*, 2014, **4**, 5870; (b) H. A. Henthorn and M. D. Pluth, *J. Am. Chem. Soc.*, 2015, **137**, 15330; (c) Z. Wu, D. Liang and X. Tang, *Anal. Chem.*, 2016, **88**, 913; (d) B. Ke, W. Wu, W. Liu, H. Liang, D. Gong, X. Hu and M. Li, *Anal. Chem.*, 2016, **88**, 592; (e) L. Wei, Z. Zhu, Y. Li, L. Yi and Z. Xi, *Chem. Commun.*, 2015, **51**, 10463.
- 12 (a) F. Yu, P. Li, P. Song, B. Wang, J. Zhao and K. Han, *Chem. Commun.*, 2012, **48**, 2852; (b) W. Sun, J. Fan, C. Hu, J. Cao, H. Zhang, X. Xiong, J. Wang, S. Cui, S. Sun and X. Peng, *Chem. Commun.*, 2013, **49**, 3890; (c) R. Wang, F. Yu, L. Chen, H. Chen, L. Wang and W. Zhang, *Chem. Commun.*, 2012, **48**, 11757; (d) Y. Zheng, M. Zhao, Q. Qiao, H. Liu, H. Lang and Z. Xu, *Dyes Pigm.*, 2013, **98**, 367.
- 13 (a) K. Sasakura, K. Hanaoka, N. Shibuya, Y. Mikami, Y. Kimura, T. Komatsu, T. Ueno, T. Terai, H. Kimura and T. Nagano, *J. Am. Chem. Soc.*, 2011, **133**, 18003; (b) H. Wu, S. Krishnakumar, J. Yu, D. Liang, H. Qi, Z.-W. Lee, L.-W. Deng and D. Huang, *Chem.-Asian J.*, 2014, **9**, 3604; (c) J. Liu, X. Guo, R. Hu, X. Liu, S. Wang, S. Li, Y. Li and G. Yang, *Anal. Chem.*, 2016, **88**, 1052.
- 14 Z. J. Huang, S. S. Ding, D. H. Yu, F. H. Huang and G. Q. Feng, *Chem. Commun.*, 2014, **50**, 9185.
- 15 (a) S. Chen, C. Ma, M.-S. Yuan, W. Wang, D.-E. Wang, S.-W. Chen and J. Wang, *RSC Adv.*, 2016, **6**, 85529; (b) H. Chen, W. Lin, H. Cui and W. Jiang, *Chem.-Eur. J.*, 2015, **21**, 733; (c) X. Cao, W. Lin, K. Zheng and L. He, *Chem. Commun.*, 2012, **48**, 10529; (d) D. Maity, A. Raj, P. K. Samanta, D. Karthigeyan, T. K. Kundu, S. K. Pati and T. Govindaraju, *RSC Adv.*, 2014, **4**, 11147.
- 16 (a) R. Y. Wang, Z. F. Li, C. Y. Zhang, Y. Y. Li, G. C. Xu, Q. Z. Zhang, L. Y. Li, L. Yi and Z. Xi, *ChemBioChem*, 2016, **17**, 962; (b) C. Wei, L. Wei, Z. Xi and L. Yi, *Tetrahedron Lett.*, 2013, **54**, 6937; (c) Y. L. Pak, J. Li, K. C. Ko, G. Kim, J. Y. Lee and J. Yoon, *Anal. Chem.*, 2016, **88**, 5476; (d) C. Wei, Q. Zhu, W. W. Liu, W. B. Chen, Z. Xi and L. Yi, *Org. Biomol. Chem.*, 2014, **12**, 479; (e) E. Karakuş, M. Üçüncü and M. Emrullahoğlu, *Anal. Chem.*, 2016, **88**, 1039.
- 17 (a) M. Marí, A. Morales, A. Colell, C. García-Ruiz, N. Kaplowitz and J. C. Fernández-Checa, *Biochim. Biophys. Acta*, 2013, **1830**, 3317; (b) G. Noctor, A. Mhamdi, S. Chaouch, Y. Han, J. Neukermans, B. Marouez-Garcia, G. Oueval and C. H. Foyer, *Plant, Cell Environ.*, 2012, **35**, 454.
- 18 (a) M. D. Slooter, K. Bierau, A. B. Chan and C. W. Löwik, *Connect. Tissue Res.*, 2015, **56**, 153; (b) M. Manley, *Chem. Soc. Rev.*, 2014, **43**, 8200.
- 19 (a) W. Sun, S. Guo, C. Hu, J. Fan and X. Peng, *Chem. Rev.*, 2016, **116**, 7768; (b) J. Yin, Y. Kwon, D. Kim, D. Lee, G. Kim, Y. Hu, J.-H. Ryu and J. Yoon, *J. Am. Chem. Soc.*, 2014, **136**, 5351; (c) A. L. Vahrmeijer, M. Hutteman, J. R. Van der Vorst, C. J. H. Van de Velde and J. V. Frangioni, *Nat. Rev. Clin. Oncol.*, 2013, **10**, 507.
- 20 A. Loudet and K. Burgess, *Chem. Rev.*, 2007, **107**, 4891.
- 21 G. L. Long and J. D. Winefordner, *Anal. Chem.*, 1983, **55**, 712A.
- 22 J. Pan and K. S. Carroll, *ACS Chem. Biol.*, 2013, **8**, 1110.
- 23 L. Yi, L. Wei, R. Wang, C. Zhang, J. Zhang, T. Tan and Z. Xi, *Chem.-Eur. J.*, 2015, **21**, 15167.
- 24 During the revision and resubmission of this manuscript (first submission on Oct. 16<sup>th</sup> 2016), a paper (*Chem. Sci.*, DOI: 10.1039/c6sc04703c) for imaging of HCT116 tumors based on H<sub>2</sub>S as a biomarker was published.

